Volume 22, No 4 | International Journal of Radiation Research, October 2024

Cone beam CT enhanced scan in evaluating the efficacy and prognosis of interventional chemoembolization and radiation for liver cancer

S. Zhao[1#], L. Wang[1#], J. Xia[1], L. Liu[2*]

[1]*Department of Radiology, the Affiliated Hospital of Shaoxing University (Shaoxing Municipal Hospital), Shaoxing 312000, Zhejiang Province, China*
[2]*Operating Room, Shaoxing People's Hospital, Shaoxing 312000, Zhejiang Province, China*

► ***Original article***

***Corresponding author:**
Lin Liu, Ph.D.,
E-mail:
shenpanpo769967401@163.com

Received: September 2023
Final revised: February 2024
Accepted: February 2024

Int. J. Radiat. Res., October 2024; 22(4): 1037-1042

DOI: 10.61186/ijrr.22.4.1037

Keywords: *Cone-beam computed tomography, hepatocellular carcinomas, transcatheter arterial chemoembolization, prognosis.*

#These authors contributed equally to this work as co-first author.

ABSTRACT

Background: This work analyzed the efficacy of Cone-Beam Computed Tomography (CBCT) enhanced scan in evaluating the therapeutic effect and prognosis of interventional therapy in patients with liver cancer (LC). ***Materials and Methods:*** Eighty-two individuals diagnosed with primary LC were enrolled here and grouped according to the intraoperative treatment. Patients in group A were only treated with digital subtraction angiography (DSA) during the operation, while those in group B received DSA and CBCT during the operation. The operation time, radiation dose, detection rate of tumor lesions, and lipiodol deposition were compared between two groups. ***Results:*** In group A, 54 lesions were identified before operation, 48 lesions during intraoperative angiography, and 6 lesions remained undetected. In group B, 57 LC lesions were identified before operation, and 57 lesions during intraoperative CBCT enhanced scan, and 2 small LC lesions not presented previously were detected. The number of lesions with complete lipiodol precipitation in group B (42) was clearly higher as against group A (32) ($P < 0.05$). The operation time of group B was clearly longer as against group A ($P < 0.05$), but there existed no substantial difference in radiation dose patients in different groups ($P > 0.05$). ***Conclusion:*** The results indicated that CBCT enhanced scan was superior to conventional DSA in detecting tumor lesions, nutrient arteries, and lipiodol deposition in patients undergoing LC chemoembolization. Importantly, this enhanced method did not increase radiation dose but prolonged the operation time.

INTRODUCTION

Liver cancer (LC) is generally divided into primary LC and secondary LC. Primary LC is cancer that forms in the liver tissue, and secondary LC is cancer that spreads to the liver from other parts of the body. Most LC cases are secondary or metastatic [1-3]. LC ranks as the third most prevalent malignant tumor, following gastric cancer and esophageal cancer, in terms of mortality rate. The initial symptoms of LC are not obvious, and the main symptoms include liver pain, fatigue, weight loss, jaundice, ascites, and other late-stage manifestations. Approximately 110,000 individuals succumb to LC annually in China, constituting 45% of global LC-related fatalities [4]. Through the monitoring of high-risk groups via serum alpha-fetoprotein (AFP) detection combined with ultrasound imaging, LC can be diagnosed at the subclinical stage, and the long-term impact of early resection becomes notably significant, leading to a clear improvement in the five-year survival rate [5]. The main cause of LC is cirrhosis caused by hepatitis B, hepatitis C or alcohol; Other causes include aflatoxin, non-alcoholic fatty liver disease and liver fluke [6,7].

Patients with early LC can choose to undergo surgery, where the surgeon has the option to either extract the entire liver or the section containing the cancer. In the case of a complete liver removal, it will be substituted with normal liver tissue obtained from a donor [8]. In addition, if laboratory tests indicate good liver function in patients with LC, and there is no evidence of cancer metastasis to nearby lymph nodes and other parts of the body, a portion of the liver can be removed. The surgeon removes the tumor and normal liver tissue around its margin together. The scope of the operation is contingent on factors such as the size, number, and location of the tumor, as well as the status of liver function [9-12]. If the tumor is diminutive, hasn't extended beyond the liver, and appropriate donor liver tissue is available, liver transplantation becomes a viable option. Donated liver tissue may originate from a deceased person or a living donor. In the case of a living donor,

[DOI: 10.61186/ijrr.22.4.1037]

the contributed tissue constitutes a segment of the liver rather than the entire organ [13]. For patients who are not suitable candidates for surgery or liver transplantation, they can choose for embolization or chemoembolization. In these procedures, a small catheter is inserted into an artery in the thigh and advanced into the hepatic artery. In embolization, doctors inject small sponges or other particles into the catheter [14].

There are many diagnostic methods for LC, including physical examination, blood test, computed tomography (CT) imaging, and MRI imaging. During a physical examination, doctors palpate the patient's abdomen to assess the liver, spleen, and other adjacent organs for any masses or alternations in shape and size, and will also inspect skin and eyes for signs of jaundice [15,16]. Several blood tests, including AFP, can be adopted to check for liver disease. High AFP level can indicate the presence of LC, and other blood tests can provide insights into the status of liver function [17,18]. Connected to a computer, an X-ray machine can acquire a sequence of intricate images depicting the liver, along with other intra-abdominal organs and blood vessels of the patient. The doctor may inject or administer contrast agents intravenously to enhance the clarity of liver imaging, providing high diagnostic accuracy [19]. A machine with a strong magnet and a computer can be adopted to take fine photos of internal areas of the body. In some cases, the use of contrast materials can enhance the clarity of the abdominal images, assisting doctors in determining the progress of LC. However, the cost of magnetic resonance imaging (MRI) scanning is high, and it is not suitable for universal application [20].

This work assessed the radiological characteristics of cone-beam computed tomography (CBCT) and the treatment mechanism of transcatheter arterial chemoembolization (TACE). This facilitated a more thorough evaluation of the vascular structure and dynamic changes in liver cancer, providing a more reliable basis for the design of individualized treatment plans. The findings opened new possibilities to enhance the post-TACE quality of life for patients with liver cancer. Therefore, this work significantly contributed to a deeper insight into the application of CBCT in TACE for liver cancer, serving as a scientific foundation for clinical practice and advancing the processes of personalization and precision in liver cancer treatment.

MATERIALS AND METHODS

Subjects

Eighty-two patients suffering from primary LC treated with interventional chemoembolization in XXX Hospital from September 2022 to May 2023 were selected as the subjects. The group comprised 49 men and 33 women, aged 41-75 years, with a mean age of 66.07 ± 7.25 years. 60 cases had a history of hepatitis, 65 cases showed elevated AFP and 21 cases had a liver surgery history. According to the intraoperative treatment, all patients were grouped. Patients in group A only underwent DSA during the operation, while those in group B underwent digital subtraction angiography (DSA) examination and CBCT scan during the operation. Participants provided written informed consent with the consent of their family members. The trial received ethical approval from the Hospital Ethics Society [Research Approval Number: IEC AF/SW-12/02.0. Ethical Approval Registration Number: 2023 (YAN)-103-01(Date: 8.13.2023). Ethics Committee Name: the Affiliated Hospital of Shaoxing University].

Inclusion criteria: Patients who had not received radiotherapy or chemotherapy; Those with complete clinical data; Patients aged above 18 years old; Patients less than 80 years old; Patients who cooperated with the examination.

Exclusion criteria: Pregnant women; Patients with other malignant tumors; Patients who dropped out of the trial; distant metastasis; Patients with severe heart disease.

Two-dimensional DSA

The procedure utilized the Siemens third-generation Artis Zee Ceiling digital subtraction angiography (DSA) machine from Germany. Following local anesthesia, percutaneous puncture of the femoral artery was performed and a 4F vascular sheath (Puncture Kit, VBM, Germany) was inserted. A 4F hepatic duct (RH catheter) (Terumo peripheral vascular imaging catheter hepatic duct, Japan) was positioned into the celiac trunk and common hepatic artery for angiography, using gadobutrol (approved by the China Food and Drug Administration, National Drug Approval H20054702, Shanghai, China) and a 2.8F microcatheter (Accessway™ Microcatheter, Jiangsu, China) was introduced into the proper hepatic artery for further angiography. The tumor nutrient arteries were evaluated based on the images obtained, and if the evaluation proved challenging, a microcatheter was positioned into the left or right hepatic artery branches for angiography.

CBCT examination

Following local anesthesia, percutaneous puncture of the femoral artery was arranged, and a 4F vascular sheath was put. Subsequently, a 4F RH catheter was positioned into the celiac trunk and common hepatic artery for angiography. Following that, CBCT angiography (Planmed, Finland) was performed. The scanning delay was set at 5 seconds, with a syringe flow rate of 1.5 mL/s. A contrast agent dose of 15 mL (gadobutrol, approved by the China Food and Drug Administration, National Drug

[DOI: 10.61186/ijrr.22.4.1037]

Approval H20054702, Shanghai, China) was administered. The scanning duration was 5 seconds, the slice thickness was 0.5mm, and the matrix size was 521×521. After confirming the tumor location, the tumor pattern was delineated on different sequences of images, and the nutrient arteries of the tumor were obtained. If no obvious enhancing lesion was identified, the tube is inserted into the suspected nutrient artery for angiography. The image diagnosis was carried out by two senior doctors, including the delineation of the tumor in the image, the identification of the feeding artery, and assessment of deposition of lipiodol on the postoperative CT.

Interventional chemoembolization

Interventional chemoembolization was performed according to the medical requirements. After identifying the nutrient artery of the patient's tumor, the microcatheter was positioned into the target vessel. Subsequently, epirubicin (Epirubicin Hydrochloride, National Drug Approval H20000496, Jiangsu, China) and a mixed emulsion of iodized oil (Iodized Oil Injection, Jiangsu, China) (at 1:2) were gradually injected under fluoroscopy. When the blood flow slowed down, an appropriate amount of sponge particles was injected, and the complete stagnation of blood flow was observed as the end point of embolization.

Statistical methods

SPSS19.0 was adopted for data analysis. Measurement data were presented as mean ± SD ($\bar{x}\pm s$), and count data were presented as percentage (%). Repeated measures analysis of variance was adopted to compare the related indicators between two groups. A two-sided test with $P < 0.05$ was considered statistically meaningful.

RESULTS

Baseline data of patients

As illustrated in figures 1-2, the mean age of patients in group A was 64.94 ± 8.25, consisting of 26 men and 15 women. Among them, 28 cases suffered from a history of hepatitis, 9 cases experienced a history of surgery and 36 and 5 cases were classified as Child-Pugh grade A and B, respectively. For tumor maximum diameter, 22 cases were < 3 cm, 15 cases were 3 - 5 cm, and 4 cases were > 5 cm. In group B, the mean age of the patients was 67.04 ± 6.81, with 23 men and 18 women. Among them, 32 cases confirmed a history of hepatitis, 12 cases reported a history of surgery, and 38 cases were classified as Child-Pugh grade A, while 3 cases were Child-Pughgrade B. For tumor maximum diameter, 24 cases were < 3 cm, 12 cases were 3 - 5 cm, and 5 cases were > 5 cm. There existed no clear difference in the average age, number of males and females, history of hepatitis, history of surgery, Child-Pugh classification, and maximum tumor diameter between patients in different groups ($P > 0.05$).

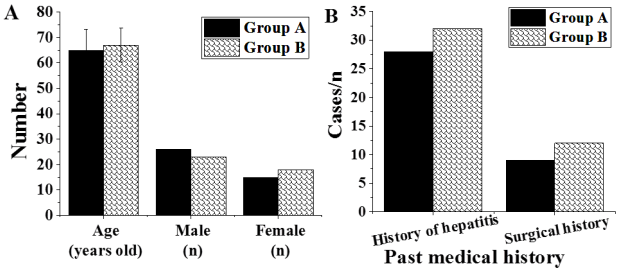

Figure 1. Mean age and the ratio of male to female of patients. **(A)**, illustrated the number of patients in groups A and B categorized by age and gender; **(B)** depicted that based on the history of hepatitis and surgery.

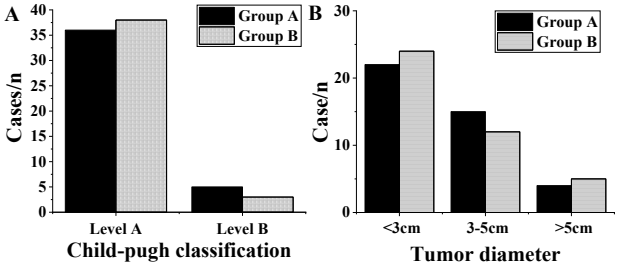

Figure 2. Child-Pugh classification and tumor maximum diameter. **(A)**, described the distribution of patients in groups A and B based on the Child-Pugh classification, where Level A corresponded to Child-Pugh A and Level B corresponded to Child-Pugh B; **(B)** illustrated the number of patients in groups A and B based on tumor diameter categories (< 3 cm, 3 - 5 cm and > 5 cm).

CT images of patients before and after treatment.

Figure 3A displayed the tumor CT scan image of a patient before he was treated, revealing a diffusely restricted lesion with low signal and the presence of a pseudocapsule. Figure 3B showcased post-treatment CT images of the patient's liver, where DWI indicated unrestrained diffusion of the lesion, presenting an isosignal.

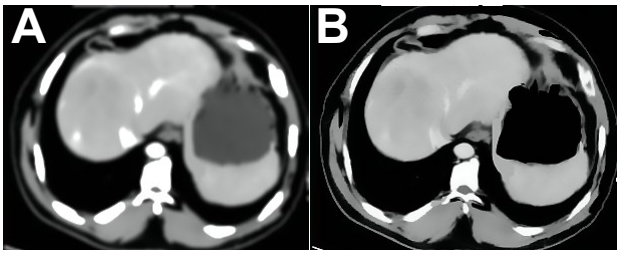

Figure 3. The tumor CT images before and after treatment. **(A)**, represented the pre-treatment liver CT image of a patient with LC. The blood flow signal in the tumor area was abnormal, characterized by large solitary low-density nodules or masses with a circular shape, and the periphery of the mass appears blurry; **(B)** shows the post-treatment liver CT image of the same LC patient, where the lesion exhibits an isosignal.

Tumor detection

As illustrated in Figure 4, utilizing the pathological diagnosis results as the gold standard, 54 lesions (31 were < 3 cm, 18 were 3 - 5 cm, and 5 were > 5 cm)

[DOI: 10.61186/ijrr.22.4.1037]

were identified in group A preoperatively, 48 lesions (26 were < 3 cm, 17 were 3 - 5 cm, and 5 were > 5 cm) were observed by intraoperative angiography, and 6 lesions were not visualized. In group B, 57 lesions were detected preoperatively (35 were < 3 cm, 15 were 3 - 5 cm, and 7 were > 5 cm), and 57 lesions were identified by intraoperative CBCT enhanced scan (35 were < 3 cm, 15 were 3 - 5 cm, and 7 were > 5 cm), and 2 small LC lesions that were not identified preoperatively were detected.

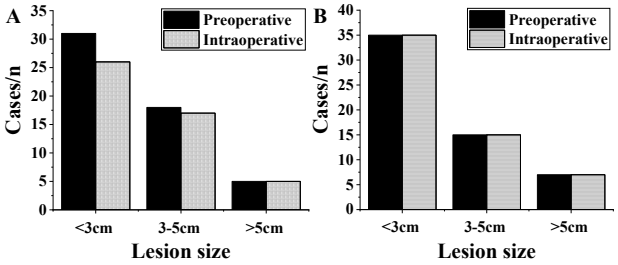

Figure 4. Tumor detection of patients. **A** and **B**: the preoperative and intraoperative examination results in groups A and B, respectively.

Results of nutrient artery assessment

Figure 5 suggested the assessment results of nutrient arteries. In group B, 125 suspected tumor-nutrient arteries were identified under routine DSA, including 121 proper hepatic arteries and 4 extrahepatic arteries. CBCT confirmed 84 tumor-nutrient arteries, including 80 proper hepatic arteries, 4 extrahepatic arteries, and 41 non-tumor-nutrient arteries. The results indicated no remarkable difference in the number of tumor-feeding arteries identified under DSA examination compared to CBCT examination, showing no visible difference ($P > 0.05$).

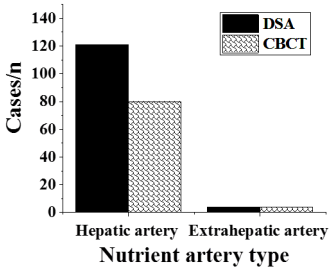

Figure 5. Results of nutrient artery assessment. The figure primarily described the number of tumor-feeding arteries identified through CBCT and DSA examinations in the patients.

Lipiodol deposition at the tumor site

Figure 6 revealed 32 lesions with complete lipiodol deposition, 17 with partial absence of lipiodol, and 5 without obvious lipiodol deposition in group A. In contrast, group B composed of 42 lesions with complete lipiodol deposition, and 15 with partial absence of lipiodol. The number of lesions with complete lipiodol precipitation in group B (42) was much higher as against group A (32) ($P < 0.05$).

Operation time and radiation dose of patients in different groups

Figure 7 suggested the operation time was 44.61±7.23 min, and the radiation dose was 205.77 ± 18.34 mGy in group A. Conversely, the operation time was 52.72 ± 6.44 min, and the radiation dose was 217.08 ± 32.65 mGy for patients in group B. The operation time of group B was longer as against group A, exhibiting a great difference ($P < 0.05$). However, similar was observed in radiation dose between patients in various groups ($P > 0.05$).

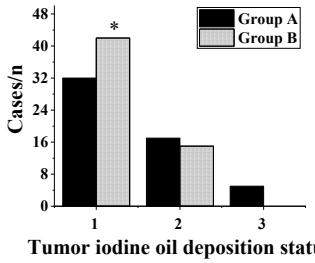

Figure 6. Lipiodol deposition in the patient's tumor. *Note: * indicated group A versus group B, P < 0.05. The figure illustrated the sedimentation status and the number of lesions in patients from groups A and B after iodized oil examination. The X-axis represented the iodized oil sedimentation conditions: 1) lesions with complete lipiodol deposition; 2) partial lipiodol absence and 3) no obvious lipiodol deposition.*

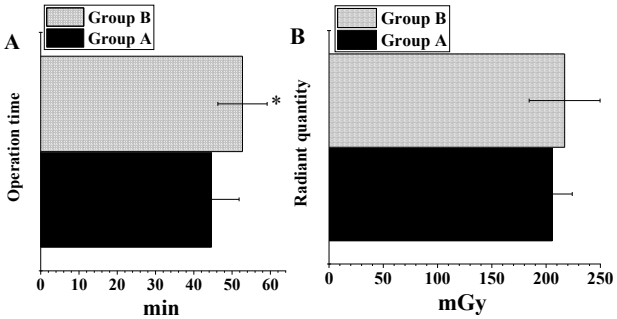

Figure 7. Contrast of operation time and radiation dose. This figure primarily depicted the differences in operation time and radiation dose between patients in different groups. Figure **A** represented the operation time and figure **B** represented the radiation dose.

DISCUSSION

LC stands among the malignant tumors with the highest global mortality and morbidity rates. Although surgical resection is the primary choice for LC treatment, only about 20% - 30% of patients can obtain the opportunity of surgical resection due to factors such as hepatitis B infection, cirrhosis, and liver insufficiency, multicentric occurrence of tumor, and early spread and metastasis in China. TACE involves the controlled injection of plugs into the supply vessels of diseased organs through arterial or intravenous catheters to cause occlusion and interrupt the blood supply. This aims to control bleeding, treat tumors and vascular lesions, and eliminate the function of diseased organs. At present, TACE or radioembolization serves as the core treatment for patients with hepatocellular LC who can't accept radical treatments like liver transplantation, tumor resection, or percutaneous radiofrequency ablation. As an auxiliary diagnostic

[DOI: 10.61186/ijrr.22.4.1037]

method for primary LC, the biggest advantage of CBCT is its fast imaging. The short scanning time reduces the image ambiguity caused by the patient's body movement and the image distortion caused by the patient's internal organ movement, thereby improving the X-ray tube efficiency [21,22]. It was observed that there was similar in the average age, number of males and females, history of hepatitis, history of surgery, Child-Pugh classification, and maximum tumor diameter between two groups (P>0.05), which provided reliability for the later study.

In this work, CBCT and DSA were employed to examine the lesion status in liver cancer patients. It can be concluded that CBCT-enhanced scanning is superior to conventional DSA in detecting tumor lesions. This superiority is attributed to the higher spatial resolution and real-time dynamic imaging advantages of CBCT, allowing for clearer visualization of small tumors or vascular abnormalities. Its three-dimensional imaging aids in a more comprehensive understanding of the tumor's condition. In contrast, DSA, with lower resolution, provides two-dimensional vascular images, which may lead to potential instances of misdiagnosis [23]. Additionally, research indicates that preoperative digital subtraction angiography can reduce the probability of postoperative bleeding [24]. In a study by Kato *et al*. (2021) [25] the combined use of CBCT and DSA revealed that three-dimensional fusion images provided clear visualization of stent and parent artery structures, demonstrating excellent diagnostic reliability. In group B, 125 suspected tumor nutrient arteries were observed under routine DSA, containing 121 proper hepatic arteries and 4 extrahepatic arteries. 84 tumor-nutrient arteries were confirmed by CBCT, containing 80 proper hepatic arteries, 4 extrahepatic arteries and 41 non-tumor-nutrient arteries. Currently, in chemoembolization treatment, the femoral artery is often cannulated to the coeliac trunk artery for angiography to determine the tumor nutrient artery and its shape, and then chemoembolization of the corresponding artery is performed [26]. Therefore, obtaining information about tumor nutrient arteries and their shape is particularly important. The above results indicate that contrast-enhanced CBCT scans are superior to conventional DSA in the detection of nutrient arteries. In investigating the application of CBCT in bronchial artery embolization and chemotherapy, studies have found that, compared to standalone DSA, CBCT enhances the credibility of tumor signal diagnosis before targeted arterial treatment [27].

In general, the interventional treatment of LC involves inserting a catheter through the patient's femoral artery to reach the blood supply site of the liver tumor. Embolic agents or chemotherapy drugs can be injected through the arteries supplying blood to the liver to delay tumor growth, thereby prolonging the survival of patients [28]. A commonly adopted embolic agent is lipiodol, as LC cells have a strong affinity for it. Interventional therapy uses lipiodol to achieve the purpose of embolization of tumor blood supply arteries [29]. The work revealed that the number of lesions with complete lipiodol deposition in Group B patients was sharply higher in contrast to that in group A patient, and it also prolonged the operation time. This finding aligns with the results of Xu R *et al*.'s research [30], indicating that the iodized oil deposition rate in patients undergoing CBCT-enhanced scans is higher than in those undergoing conventional DSA angiography. However, the radiation dose for patients in the CBCT-enhanced scan group does not increase; it only extends the operation time. This suggests that, while obtaining more treatment information, the study aims to ensure the effectiveness of treatment and the safety of radiation.

In summary, when compared to standalone DSA, the combination of CBCT and DSA demonstrates a notable enhancement in the detection performance of tumor lesions, feeding arteries, and iodized oil deposition in patients undergoing chemoembolization for liver cancer. It enhances the detection rate of tumor lesions and related arterial abnormalities, all while maintaining a comparable radiation dose, thus ensuring good safety during treatment.

CONCLUSION

The results of this work indicated that CBCT-enhanced scanning outperforms conventional DSA angiography in detecting tumor lesions, feeding arteries, and iodized oil deposition in patients undergoing chemoembolization for liver cancer. It provided a more comprehensive and accurate diagnosis of the vascular structure and dynamic changes in liver cancer, offering new possibilities for improving the efficacy of TACE treatment and the quality of life for patients. This work also suggested that the combination of CBCT and DSA application prolongs the operation time without increasing the radiation dose. However, it was essential to note that the sample size was small and comes from a single source, which may introduce some bias to the results. Additionally, this work lacked follow-up records on the occurrence of complications after chemoembolization, and there is a shortage of corresponding prognosis data for analysis.

ACKNOWLEDGMENT

None.

Ethical consideration: All individuals and/or their parents have provided informed consent to

[DOI: 10.61186/ijrr.22.4.1037]

participate in this study, and the study has been approved by the Affiliated Hospital of Shaoxing University Medical Research Ethics Committee, Registration Number: 2023(YAN)-103-01 (Date: 8.13.2023).

Conflict of interest: The authors declare no competing interests.

Funding: Not applicable.

Author Contributions: S.Z., L.W., J.X. and L.L.; drafting/revision of the manuscript for content and including medical writing for content and article frame design All authors contributed to the article and approved the submitted version.

REFERENCES

1. Singh S, Chaurasia A, Gopal N, Malayeri A, Ball MW (2022) Treatment strategies for hereditary kidney cancer: Current recommendations and updates. *Discov Med,* ***34(173)****: 205-220. PMID: 36602871.*
2. Li CX, Chen B, Yu H, Zhang YG (2023) LncRNA DNM3OS Promotes tumorigenesis of liver cancer by inducing FOXO3a methylation via interacting with DNMT1. *Journal of Biological Regulators and Homeostatic Agents,* ***37(1)****: 111-120.*
3. Feng W, Wang Q, Wang S, Chen Z, Lin B (2022) Effect of indocyanine green (icg)-mediated near-infrared light guided liver tumor resection on the prognosis of patients with primary liver cancer. *Acta Medica Mediterranea,* ***38:*** *4061.*
4. Zhu, R, Du T, Gao H (2020) Effects of dezocine and ropivacaine infiltration anesthesia on cellular immune function indicators, anesthesia recovery time and pain factors in patients with open liver resection. *Cellular and Molecular Biology,* ***66(3):*** *149-154.*
5. Marengo A, Rosso C, Bugianesi E (2016) Liver cancer: Connections with obesity, fatty liver and cirrhosis. *Annu Rev Med,* ***67:*** *103-117.*
6. Anwanwan D, Singh SK, Singh S, Saikam V, Singh R (2020) Challenges in liver cancer and possible treatment approaches. *Biochim Biophys Acta Rev Cancer,* ***1873(1):*** *188314.*
7. Li X, Ramadori P, Pfister D, Seehawer M, Zender L, Heikenwalder M (2021) The immunological and metabolic landscape in primary and metastatic liver cancer. *Nat Rev Cancer,* ***21(9):*** *541-557.* doi: 10.1038/s41568-021-00383-9. Epub 2021 Jul 29. PMID: 34326518.
8. Zheng Y, Wang S, Cai J, Ke A, Fan J (2021) The progress of immune checkpoint therapy in primary liver cancer. *Biochim Biophys Acta Rev Cancer,* ***1876(2):*** *188638.* doi: 10.1016/j.bbcan.2021.188638. Epub 2021 Oct 22. PMID: 34688805.
9. Bhardwaj H, Tomar P, Sakalle A, Bhardwaj A, Asthana R, Vidyarthi A (2023) EEG based personality prediction using genetic programming. *Wiley,* ***2023:*** *1-13.*
10. Gao S, Gang J, Yu M, Xin G, Tan H (2021) Computational analysis for identification of early diagnostic biomarkers and prognostic biomarkers of liver cancer based on GEO and TCGA databases and studies on pathways and biological functions affecting the survival time of liver cancer. *BMC Cancer,* ***21(1):*** *791.* doi: 10.1186/s12885-021-08520-1. PMID: 34238253; PMCID: PMC8268589.
11. Huang J, Wang L, Siddik A B, Abdul-Samad Z, Bhardwaj A, Singh B (2023) Forecasting GHG emissions for environmental protection with energy consumption reduction from renewable sources: A sustainable environmental system. *Ecological Modelling,* ***475:*** *110181.*
12. Shiani A, Narayanan S, Pena L, Friedman M (2017) The Role of Diagnosis and Treatment of Underlying Liver Disease for the Prognosis of Primary Liver Cancer. *Cancer Control,* ***24(3):*** *1073274817729240.* doi: 10.1177/1073274817729240. PMID: 28975833; PMCID: PMC5937237.
13. Wege H, Schulze K, von Felden J, Calderaro J, Reig M (2021) Rare liver tumors working group of the European Reference Network on Hepatological Diseases (ERN RARE-LIVER). Rare variants of primary liver cancer: Fibrolamellar, combined, and sarcomatoid hepatocellular carcinomas. *Eur J Med Genet,* ***64(11):*** *104313.* doi: 10.1016/j.ejmg.2021.104313. Epub 2021 Aug 18. PMID: 34418585.
14. Gao YX, Yang TW, Yin JM, Yang PX, Kou BX, Chai MY, *et al*. (2020) Progress and prospects of biomarkers in primary liver cancer (Review). *Int J Oncol,* ***57(1):*** *54-66.* doi: 10.3892/ijo.2020.5035. Epub 2020 Apr 1. PMID: 32236573.
15. Wang J, Liu X, Jin T, Cao Y, Tian Y, Xu F (2022) NK cell immunometabolism as target for liver cancer therapy. *Int Immunopharmacol,* ***112:*** *109193.* doi: 10.1016/j.intimp.2022.109193. Epub 2022 Sep 7. PMID: 36087507.
16. Krishan A and Mittal D (2021) Ensembled liver cancer detection and classification using CT images. *Proc Inst Mech Eng H,* ***235(2):*** *232-244.* doi: 10.1177/0954411920971888. Epub 2020 Nov 13. PMID: 33183141.
17. Rahimi A, Khalil A, Faisal A, Lai KW (2022) CT-MRI Dual Information Registration for the Diagnosis of Liver Cancer: A Pilot Study Using Point-based Registration. *Curr Med Imaging,* ***18(1):*** *61-66.* doi: 10.2174/1573405617666210825155659. PMID: 34433403.
18. Kumar A, Sinha N, Bhardwaj A, Goel S (2022) Clinical risk assessment of chronic kidney disease patients using genetic programming. *Computer Methods in Biomechanics and Biomedical Engineering,* ***25(8):*** *887-895.*
19. Ayuso C, Rimola J, Vilana R, Burrel M, Darnell A, García-Criado Á, *et al*. (2018) Diagnosis and staging of hepatocellular carcinoma (HCC): current guidelines. *Eur J Radiol,* ***101:*** *72-81.* doi: 10.1016/j.ejrad.2018.01.025. Epub 2018 Jan 31. Erratum in: Eur J Radiol. 2019 Mar; 112:229. PMID: 29571804.
20. Feng YS, Zhou JM, Sun CH, Zhu J, Yang J, Guo L (2021) The diagnostic value of miR-21 combined with CT in patients with liver cancer. *Clin Transl Oncol,* ***23(6):*** *1238-1244.* doi: 10.1007/s12094-020-02514-4. Epub 2020 Nov 18. PMID: 33206331.
21. Luz JHM, Veloso Gomes F, Costa NV, Vasco I, Coimbra E, Luz PM, *et al*. (2021) BestFLR Trial: Liver Regeneration at CT before Major Hepatectomies for Liver Cancer-A Randomized Controlled Trial Comparing Portal Vein Embolization with N-Butyl-Cyanoacrylate Plus Iodized Oil versus Polyvinyl Alcohol Particles Plus Coils. *Radiology,* ***299(3):*** *715-724.* doi: 10.1148/radiol.2021204055. Epub 2021 Apr 6. PMID: 33825512.
22. Turukmane AV, Alhebaishi N, Alshareef AM, Mirza OM, Bhardwaj A, Singh B (2022) Multispectral image analysis for monitoring by IoT based wireless communication using secure locations protocol and classification by deep learning techniques. *Optik,* ***271:*** *170122*
23. Ebadi N, Li R, Das A, Roy A, Nikos P, Najafirad P (2023) CBCT-guided adaptive radiotherapy using self-supervised sequential domain adaptation with uncertainty estimation. *Med Image Anal,* ***86:*** *102800.* doi: 10.1016/j.media.2023.102800. Epub 2023 Mar 16. PMID: 37003101.
24. Stefanelli A, Sabourin V, Hines K, Matias C, Acharya S, Sharan A, *et al*. (2022) Digital subtraction angiography may reduce the rate of radiographic hemorrhage in stereoelectroencephalography. *World Neurosurg,* ***164:*** *e964-e969.* doi: 10.1016/j.wneu.2022.05.081. Epub 2022 May 25. PMID: 35643404.
25. Kato N, Yuki I, Otani K, Ishibashi T, Kakizaki S, Nagayama G, *et al*. (2021) Flow diverter apposition in patients with large or giant intracranial aneurysms evaluated on three-dimensional fusion images acquired by high-resolution cone-beam computed tomography and digital subtraction angiography. *World Neurosurg,* ***147:*** *e388-e395.* doi: 10.1016/j.wneu.2020.12.068. Epub 2021 Jan 7. PMID: 33359518.
26. Kong Y, Jing Y, Sun H, Zhou S (2022) The diagnostic value of contrast-enhanced ultrasound and enhanced ct combined with tumor markers afp and ca199 in liver cancer. *J Healthc Eng,* ***2022:*** *5074571.* doi: 10.1155/2022/5074571. PMID: 35237392; PMCID: PMC8885265.
27. Liu MY, Rose SC, Loh A, Taddonio M, Redmond JW, Meisinger QC, *et al*. (2022) Utility of cone-beam ct for bronchial artery embolization and chemoinfusion: a single-institution retrospective case series. *Cardiovasc Intervent Radiol,* ***45(6):*** *834-840*. doi: 10.1007/s00270-022-03148-5. Epub 2022 Apr 19. PMID: 35441243; PMCID: PMC9117382.
28. Su Y, Liu S, Guan Y, Xie Z, Zheng M, Jing X (2020) Renal clearable Hafnium-doped carbon dots for CT/Fluorescence imaging of orthotopic liver cancer. *Biomaterials,* ***255:*** *120110.* doi: 10.1016/j.biomaterials.2020.120110. Epub 2020 Jun 8. PMID: 32540755.
29. Zhu H, Wang DD, Yuan T, Yan FJ, Zeng CM, Dai XY, *et al*. (2018) Multikinase inhibitor CT-707 targets liver cancer by interrupting the hypoxia-activated IGF-1R-YAP axis. *Cancer Res,* ***78(14):*** *3995-4006.* doi: 10.1158/0008-5472.CAN-17-1548. Epub 2018 Apr 18. PMID: 29669759.
30. Xu R, Wang J, Huang X, Zhang Q, Xie Y, Pang L, *et al*. (2019) Clinical value of spectral CT imaging combined with AFP in identifying liver cancer and hepatic focal nodular hyperplasia. *J BUON,* ***24(4):*** *1429-1434*. PMID: 31646787.

[DOI: 10.61186/ijrr.22.4.1037]